Original paper

Manganrockbridgeite from the Jocão claim, Conselheiro Pena, Minas Gerais, Brazil: chemistry, spectroscopic and structural data

Jaromír TVRDÝ[1,2]*, Luboš VRTIŠKA[2], Jan FILIP[3], Zdeněk DOLNÍČEK[2], Radek ŠKODA[1], Martin PETR[3] and Radana MALÍKOVÁ[1,2]

[1] *Department of Geological Sciences, Faculty of Science, Masaryk University, Kotlářská 2, 61137 Brno, Czech Republic; jt.geologie@gmail.com*
[2] *Department of Mineralogy and Petrology, National Museum, Cirkusová 1740, 19300 Praha 9, Czech Republic*
[3] *Regional Centre of Advanced Technologies and Materials, Czech Advanced Technology and Research Institute, Palacký University, Šlechtitelů 27, 78371 Olomouc, Czech Republic*
**Corresponding author*

The world's second occurrence of the recently described manganrockbridgeite was found in a mineral assemblage in the Jocão (Cigana) pegmatite, Conselheiro Pena district, Minas Gerais (Brazil). Manganrockbridgeite forms green botryoidal--crystalline crusts with a velvety surface covering the walls of leached cavities in triphylite replaced by correianevesite and Mn-rich vivianite. The outer zone is significantly richer in Mn than the inner zone where the manganrockbridgeite passes to frondelite. Other associated minerals are hureaulite and kenngottite-like phosphate. Empirical formulae based on EPMA, Mössbauer and XPS spectroscopy are $(Mn_{1.36}Fe^{2+}_{0.46}Fe^{3+}_{0.09}Ca_{0.03}Mg_{0.01}\square_{0.05})_{\Sigma 2.00}Fe^{3+}_{2.95}(PO_4)_{3.00}(OH)_{3.84}(H_2O)_{1.16}$ for the outer zone and $(Mn_{1.03}Fe^{2+}_{0.49}Fe^{3+}_{0.29}Ca_{0.03}Mg_{0.02}\square_{0.14})_{\Sigma 2.00}Fe^{3+}_{2.94}(PO_4)_{3.00}(OH)_{3.81}(H_2O)_{1.19}$ for the inner zone of aggregates. Raman spectra and assignment of individual decomposed bands to vibrational modes show a good agreement with data published for frondelite from the Jocão locality. Powder diffraction data of the studied manganrockbridgeite correspond to the type material from Hagendorf-Süd, Germany. Unit-cell parameters for space group $P2_1/m$ are a = 5.195(2) Å, b = 16.936(4) Å, c = 7.452(2) Å, β = 110.25(3)° and V = 615.1(4) Å^3.

Keywords: manganrockbridgeite, phosphate minerals, Jocão pegmatite, Minas Gerais, Brazil
Received: 2 October 2023; accepted: 3 April 2024; handling editor: M. Števko

1. Introduction

Minerals of the recently approved rockbridgeite group have a structure-based formula $A_2B_3(PO_4)_3(OH, H_2O)_5$, where *A* corresponds to the *M*2 site and contains all divalent cations and *B* includes the 1× *M*1 and 2× *M*3 sites dominated usually by Fe^{3+}. The charge balance caused by the presence of trivalent and divalent cations in this site is balanced by the substitution of OH^- for H_2O (Grey et al. 2019b). The different group members are distinguished by the occupancy of the *A* position (i.e. the *M*2 site; Tab. 1).

A triangular discrimination diagram with five fields has been introduced for the Fe^{2+}, Mn^{2+} and Fe^{3+} dominated phases. While rockbridgeite and frondelite are minerals known for a long time (Frondel 1949; Lindberg 1949), both ferrorockbridgeite and ferrirockbridgeite have been defined in the context of the new classification scheme (Grey et al. 2019a, b). The last player in this triangle court, manganrockbridgeite, was recently approved under IMA No. 2022-122. The holotype specimen comes from the Hagendorf-Süd pegmatite mine, Upper Palatinate, Bavaria, Germany, a classic locality of phosphate minerals. Manganrockbridgeite occurs there in association with frondelite, kenngottite, hureaulite and hematite. Other identified minerals include quartz, correianevesite, tavorite, switzerite, bermanite, jahnsite-

Tab. 1 Ideal formulae, space group (SG), and unit-cell parameters for rockbridgeite-group minerals (Grey et al. 2023)

Mineral	Formula	SG	*a*	*b*	*c*	β	V, Å^3	Reference
Rockbridgeite	$(Fe^{2+}_{0.5}Fe^{3+}_{0.5})_2Fe^{3+}_3(PO_4)_3(OH)_5$	*Bbmm*	13.783	16.805	5.172		1198.0	Moore (1970)
Frondelite	$(Mn^{2+}_{0.5}Fe^{3+}_{0.5})_2Fe^{3+}_3(PO_4)_3(OH)_5$	*Bbmm*	13.89	17.01	5.21		1231.0	Lindberg (1949)
Ferrorockbridgeite	$Fe^{2+}_2Fe^{3+}_3(PO_4)_3(OH)_4(H_2O)$	*Bbmm*	14.008	16.808	5.190		1222.0	Grey et al. (2019a)
Ferrirockbridgeite	$(Fe^{3+}_{0.67}\square_{0.33})_2Fe^{3+}_3(PO_4)_3(OH)_4(H_2O)$	*Bbmm*	13.853	16.928	5.192		1217.5	Grey et al. (2019b)
Manganrockbridgeite	$Mn^{2+}_2Fe^{3+}_3(PO_4)_3(OH)_4(H_2O)$	$P2_1/m$	5.198	16.944	7.451	110.17	616.0	Grey et al. (2023)
Plimerite	$Zn_2Fe^{3+}_3(PO_4)_3(OH)_4(H_2O)$	*Bbmm*	13.865	16.798	5.151		1199.7	Elliott et al. (2009)

group minerals, stewartite, laueite and pseudolaueite (Grey et al. 2023).

Manganese-rich frondelite identical to manganrockbridgeite was identified on a sample from the Jocão claim, Conselheiro Pena County, Minas Gerais (Brazil) in an assemblage of secondary phosphate minerals. This paper presents the results of a detailed study of this specimen, including new spectroscopic data and a comparison with the original material.

2. Occurrence, mineral assemblage and sample description

The Jocão (also called Cigana) pegmatite (19.0758975S, 41.4954067W) is located in the Conselheiro Pena district of the Eastern Brazilian Pegmatite Province, about 17 km from the municipality of Galiléia in the state of Minas Gerais (Pedrosa-Soares et al. 2011). The pegmatite body, more than 50 m long and up to 20 m thick, penetrates quartz–biotite schists of Neoproterozoic age. It has been mined since the 1960s for industrial feldspar, spodumene, beryl and mineral specimens for the collectors' market. The locality is known worldwide for the occurrence of secondary phosphates originated by the alteration of primary triphylite. Currently, more than 50 phosphate minerals are known from the locality (Mindat.org 2023), mainly correianevesite, eosphorite, fairfieldite, fluorapatite, frondelite, gormanite, hureaulite, lithiophyllite and vivianite (Chaves et al. 2005; Pedrosa-Soares et al. 2009, 2022). Correianevesite, a $Fe^{2+}Mn^{2+}$ member of the phosphoferrite–reddingite series was first described from the Jocão pegmatite (Chukanov et al. 2014).

Minerals of the rockbridgeite–frondelite series occurring in three types of phosphate associations after altered triphylite in the Jocão pegmatite were studied by Baijot et al. (2014). They appear as fibrous, radially arranged aggregates of dark green, brown or orange colour, commonly associated with barbosalite, hureaulite, tavorite and members of the jahnsite group. The electron-microprobe compositions showed a variation of 4–11 wt. % MnO and 40–50 wt. % FeO_{tot}. Rockbridgeite from the Jocão pegmatite containing 1.70–3.37 wt. % MnO was also described as an alteration product of barbosalite by Ardizzi and Atencio (2018).

Fig. 1. A dissolution cavity in brown correianevesite covered with a crust of green manganrockbridgeite and crystals of light pink hureaulite. Photo by Luboš Vrtiška.

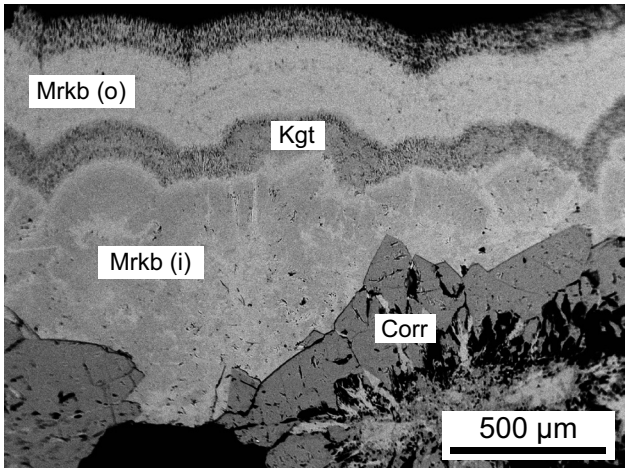

Fig. 2. Two zones of manganrockbridgeite (Mrkb) separated by a phase close to kenngottite (Kgt) grow sharply on correianievesite (Corr). The outer zone (o) appears lighter than the inner zone (i) due to the higher Mn/Fe ratio, and passes into a porous crystalline aggregate at the surface. BSE image by Zdeněk Dolníček.

The mineral assemblage examined is different from those described above. The 8.5 × 7 × 4 cm specimen consists of grey triphylite, partly replaced by cinnamon brown correianevesite and dark blue vivianite, with abundant corrosion cavities. The cavities are covered with brown crystals of correianevesite, pink hureaulite and crusts of frondelite–manganrockbridgeite, often with a velvety surface (Fig. 1). The crusts generally consist of two layers, the older greenish black and the younger paler green, separated by a yellowish acicular-porous zone of kenngottite-like mineral (Fig. 2). This mineral could not be accurately identified due to its high porosity and weak crystallinity, but it is very similar in appearance and chemistry to the Hagendorf-Süd kenngottite described by Keck et al. (2022) in an analogous association. In addition, several isolated small cavities almost filled with crystalline greenish frondelite occur in the studied sample. Supergene phosphates containing "foreign" cations are not present.

3. Results

3.1. Mössbauer spectroscopy

The bulk Fe^{3+}/Fe_{tot} ratio, as well as assignment of iron to particular structural sites, was determined from Mössbauer spectroscopy. The transmission ^{57}Fe Mössbauer spectrum was collected at room temperature using a

Tab. 2 Mössbauer parameters for manganrockbridgeite from the Jocão pegmatite

Component	Spectral area [%]	Isomer shift [mm/s]	Quadrupole splitting [mm/s]
D1 – Fe^{3+}	72.3	0.40	0.48
D2 – Fe^{3+}	14.6	0.45	0.79
D3 – Fe^{2+}	13.1	1.05	2.95

conventional Mössbauer spectrometer (MS2006 type based on virtual instrumentation technique; Pechoušek et al. 2012) in transmission geometry (constant acceleration mode) with a ^{57}Co (in Rh matrix) radioactive source (1.85 GBq) and fast scintillation detector with a $YAlO_3$:Ce crystal (Physical Electronics; Regional Centre of Advanced Technologies and Materials, Palacký University Olomouc). Carefully hand-picked crystal aggregates of manganrockbridgeite (mixed inner and outer zone) were ground under isopropyl alcohol to avoid possible iron oxidation. The hyperfine parameters were calibrated against a rolled metallic iron (α-Fe) foil at room temperature. The spectrum was fitted by Lorentz functions using the CONFIT2000 software (Žák and Jirásková 2006). The experimental error is ± 0.02 mm/s for the hyperfine parameters and ± 3 % for the relative spectral areas.

The Mössbauer spectrum of manganrockbridgeite from the Jocão pegmatite was fitted by three Lorentzian doublets (in a similar way as in the study of Redhammer et al. 2006; see Fig. 3), two with hyperfine parameters typical for Fe^{3+} and one ascribed to Fe^{2+}, giving the atomic ratio (i.e., ratio of corresponding spectral areas) 86.9 % Fe^{3+} to 13.1 % Fe^{2+} (Tab. 2).

Greenish brown frondelite from separate cavities was not analysed by Mössbauer spectroscopy. The Fe^{2+}/Fe^{3+} ratio was estimated consistently with the value found by Grey et al. (2019a) for the type frondelite from the Sapucaia locality, where the mineral occurs in a similar paragenesis.

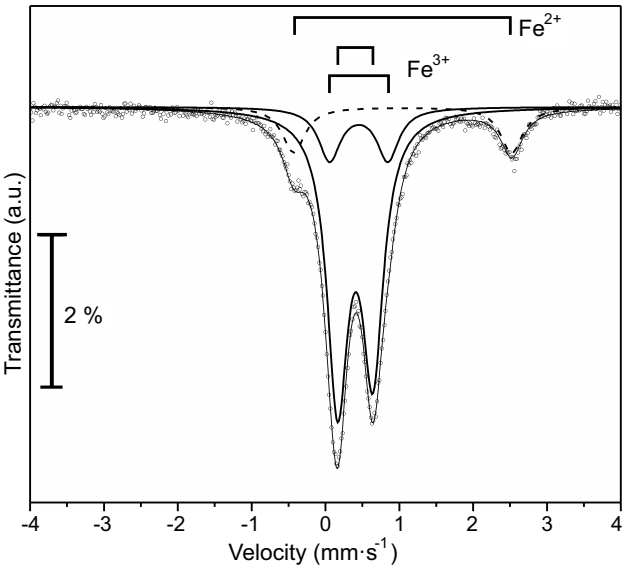

Fig. 3. Fitted Mössbauer spectrum for manganrockbridgeite from the Jocão pegmatite.

3.2. X-ray photoelectron spectroscopy

The relative proportion of divalent and trivalent iron in manganrockbridgeite from the Jocão pegmatite determined by Mössbauer spectroscopy was tentatively verified by X-ray photoelectron spectroscopy (XPS) on small areas. The measurements were performed the PHI 5000 VersaProbe II XPS system (Physical Electronics; Regional Centre of Advanced Technologies and Materials, Palacký University Olomouc) using a monochromatic Al K_α source (15 kV and 50 W) and photon energy of 1486.7 eV. All the spectra were measured in a vacuum of 1.1×10^{-7} Pa and at a temperature of 21 °C. The analysed area on the sample was a spot 100 μm in diameter. The high-resolution spectra were measured with pass energy of 23.500 eV and step of 0.2 eV. Dual-beam charge compensation was used for all measurements. All binding energy values were referenced to the carbon peak C 1s at 284.80 eV. Data were analysed with MultiPak (Ulvac-PHI, Inc.) software version 9.9.0.8 using Gaussian–Lorentzian function with iterated Shirley routine background subtraction (Shirley 1972).

Generally, *p* orbitals exhibit spin-orbit splitting in XPS. The spin-orbit splitting is projected as a doublet in the

Tab. 3 Estimation of a relative content of Fe^{2+} based on the area of the peak Fe $2p_{3/2}$(1) for manganrockbridgeite from the Jocão pegmatite in comparison with selected iron phosphates (data from Tvrdý et al. 2022)

Mineral, locality, ideal formula	Peak	Binding energy (eV)	Area (%)	Fe^{2+} (%)
Manganrockbridgeite	(1)	709.2	2.4	~ 14
Jocão claim, Minas Gerais, Brazil	(2)	711.7	83.0	
$Mn^{2+}{}_2Fe^{3+}{}_3(PO_4)_3(OH)_4(H_2O)$	(3)	713.9	14.6	
Beraunite	(1)	709.4	1.2	~ 0
Hrbek mine, Bohemia, Czech Republic	(2)	711.7	62.9	
$Fe^{3+}{}_6(PO_4)_4O(OH)_4 \cdot 6H_2O$	(3)	713.5	35.9	
Ferroberaunite	(1)	708.6	2.2	~ 12
Gravel Hill mine, Cornwall, UK	(2)	710.8	76.1	
$Fe^{2+}Fe^{3+}{}_5(PO_4)_4(OH)_5 \cdot 6H_2O$	(3)	713.0	21.8	
Vivianite	(1)	709.3	8.8	~ 92
Roșia Poieni, Alba, Romania	(2)	711.0	59.3	
$Fe^{2+}{}_3(PO_4)_2 \cdot 8H_2O$	(3)	713.8	31.9	
Childrenite	(1)	709.0	9.5	~ 100
George & Charlotte mine, Devon, UK	(2)	710.9	64.9	
$Fe^{2+}Al(PO_4)(OH)_2 \cdot H_2O$	(3)	714.0	25.6	

XPS spectrum (Briggs 2003). In the Fe 2p region, there is significant splitting of the Fe $2p_{3/2}$ and Fe $2p_{1/2}$ components (~13 eV) with the ratio 2 : 1, respectively. Other spectral features in this region are shake-up lines caused by a finite probability that the ion will be left in an excited state a few electronvolts above the ground state. This leads to the formation of satellite peaks (Moulder et al. 1995).

Because the procedure for accurately fitting the Fe 2p region is very complex, the simplifying procedure used by Kloprogge and Wood (2020) for natural mineral phases and subsequently applied by Tvrdý et al. (2022) was chosen. To estimate the valence states of iron, an empirical approach comparing Fe $2p_{3/2}$ spectra with standards was used, which avoids having to describe the peak shapes analytically (e.g. Rhodes 2021). Studied manganrockbridgeite (outer zone) was compared with the pattern of beraunite, ferroberaunite, vivianite and childrenite. High-resolution spectra for the 707–717 eV binding energy section decomposed to three main peaks for Fe $2p_{3/2}$ are shown in Fig. 4. A tentative ratio $Fe^{2+}/(Fe^{2+}+Fe^{3+})$ estimated from the relative area of the peak Fe $2p_{3/2}(1)$ and the corresponding regression curve is given in Tab. 3. The observed value of approximately 14 % Fe^{2+} is close to that of ferroberaunite and corresponds to the value obtained by Mössbauer spectroscopy (13.1 %).

3.3. Raman spectroscopy

Raman spectra of studied samples were collected in the range 4500–70 cm^{-1} using a DXR dispersive Raman Spectrometer (Thermo Scientific) mounted on a confocal Olympus microscope. The Raman signal was excited by an unpolarised 532 nm diode-pumped solid-state laser and detected by a CCD detector (size 1650 × 200 mm, Peltier cooled to –60 °C, quantum efficiency 50 % and dynamic range 360–1100 nm). The experimental parameters were: 50 × objective, 10 s exposure time, 360 exposures, 50 µm pinhole spectrograph aperture and 4 mW laser power level (estimated resolution 8.1–18.7 cm^{-1}, estimated spot size 1.1 µm). The spectra were repeatedly acquired from different parts of the sample in order to obtain a representative spectrum with the best signal-to-noise ratio. The possible thermal damage of the measured point was excluded by visual inspection of the exposed surface after measurement, by observation of possible decay of spectral features at the start of excitation and checking for thermal

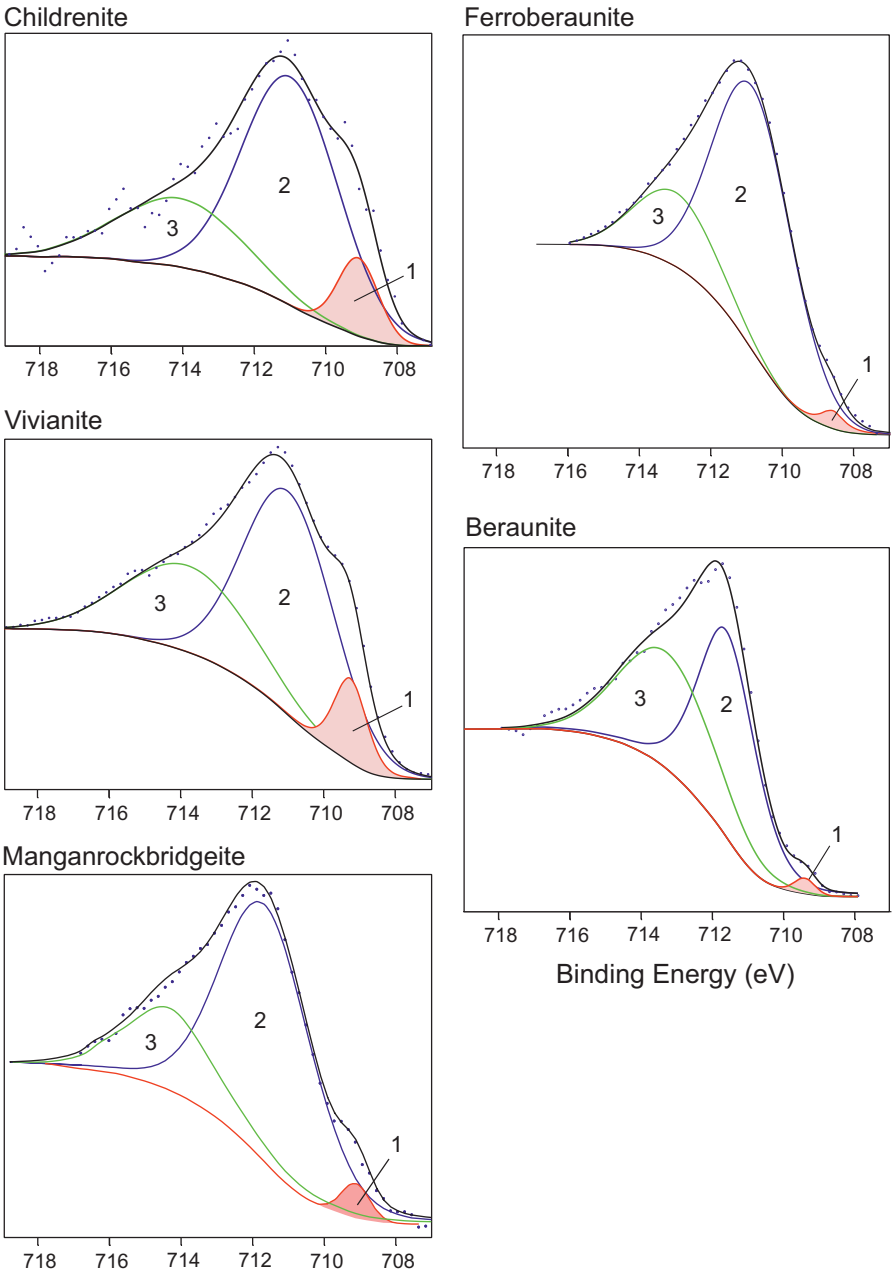

Fig. 4. Comparison of high-resolution Fe $2p_{3/2}$ XPS spectra of manganrockbridgeite from the Jocão pegmatite with the patterns of ferric (beraunite), ferrous-ferric (ferroberaunite) and ferrous phosphates (vivianite and childrenite) given in Tvrdý et al. (2022). The numbering of peaks corresponds to Tab. 3; the peaks Fe $2p_{3/2}$ (1) used to estimate a relative content of Fe^{2+} are highlighted.

Tab. 4 Tentative assignment of Raman spectrum of manganrockbridgeite in comparison with frondelite from the Jocão pegmatite

Manganrockbridgeite (new data)				Frondelite (Frost *et al.* 2013)		Tentative assignment
Center [cm^{-1}]	FWHM [cm^{-1}]	$I_{rel.}$ (height) [%]	$I_{rel.}$ (area) [%]	Center* [cm^{-1}]	$I_{rel.}$ (area)* [%]	
3574	19	21	9	3581	11	ν O-H stretch of hydrogen bonded water molecules
3392	87	6	13	3315	61	OH stretching vibrations
3322	90	4	9	3144	9	
3254	165	4	18	3029	12	
				2866	44	
				2747	23	
1587	147	2	8	1597	23	bending mode of non-hydrogen bonded water
				1532	16	
				1532	20	
				1416	2	
1183	37	6	5	1164	29	ν_3 and ν_1 PO_4 stretching region
1147	36	17	15	1112	18	
1109	37	58	51	1071	100	
1053	53	77	100	1027	77	
998	35	43	37	1000	45	
960	21	100	51	966	41	
943	42	18	18			
701	45	7	7	748	18	Water librational modes
632	17	4	2	635	4	ν_4 PO_4 bending modes
612	18	12	5	612	32	
580	27	44	29	589	3	
				572	16	
517	25	6	4	481	28	ν_2 PO_4 bending modes
495	22	11	6	455	19	
463	37	85	76	436	9	
445	19	27	12			
431	25	43	27			
407	12	5	2			
381	34	27	23	379	9	metal-oxygen vibrations
355	34	12	8	329	44	
317	54	44	59			
280	32	18	15			
263	20	12	7			
234	25	32	20			overlapping with lattice modes
176	20	2	1			lattice and other modes
153	17	23	7			
142	28	24	14			
124	14	25	7			
109	24	33	19			
94	13	36	11			
74	14	52	20			
60	5	13	1			

* Values derived from deconvoluted spectra.

downshift of Raman lines. The instrument was set up by a software-controlled calibration procedure using multiple neon emission lines (wavelength calibration), multiple polystyrene Raman bands (laser-frequency calibration) and standardized white-light sources (intensity calibration). Spectral manipulations were performed using the Fityk software (Wojdyr 2010). A Gaussian/Lorentz (pseudo-Voigt) function was used to obtain the band components of the spectra; the resulting squared correlation coefficient R^2 between the observed and calculated profiles yielded 0.998.

Raman spectra obtained for the inner and outer zones of manganrockbridgeite aggregates (ESM 1, 2; measuring points nearby #7 and #37 of EPMA in ESM 3) show a very good agreement (Fig. 5). Both records correspond to frondelite from Jocão containing an average Mn content of 0.68 *apfu* calculated on the basis of 17 oxygen atoms in the structure (Frost et al. 2013).

The band wavenumbers obtained by decomposition of the Raman spectrum of the outer manganrockbridgeite zone and their assignment to vibrational states are given in Tab. 4. According to Grey et al. (2023), the crystal structure of manganrockbridgeite is dominated by trimers of face-sharing *M*1- and *M*2-centred octahedrons. The trimers are connected into chains along [010] by edge-sharing between the *M*2-centred octahedra and into (001) planes by corner-sharing with PO_4 tetrahedra. These planes alternate with 001 planes containing dimers of corner-connected *M*3-centred octahedra that share faces along [100]. In the $P2_1/m$ structure the *M*3 sites are split into pairs of sites, *M*3a and *M*3b. The presence of hydroxyl ions is assumed at sites in the vertices of shared coordination octahedra. A substitution of H_2O for OH^- is expected to maintain charge balance in the empirical formula. The point at which the Raman spectrum was measured corresponds to chemical analysis #7 in the Supplement. Values of 4.29 apfu OH^- and only 0.71 apfu H_2O can be expected here.

In the 4000–3000 cm^{-1} region, the spectrum is shaped by bands caused by OH stretching vibrations (Fig. 6a). The sharp peak at 3574 cm^{-1} is attributed to the OH^- groups in the crystal structure. The broad hump caused by the bands at 3392, 3322 and 3254 cm^{-1} could be assigned to the ν_1 and ν_3 OH stretching vibrations of the molecular H_2O. The relatively weak range compared to the data for frondelite of Frost et al. 2013 (Tab. 4) may reflect a low proportion of H_2O in the structure. Similarly, the effect of the bending mode of non-hydrogen bonded water at 1800–1400 cm^{-1} is reduced in the studied sample. In the PO_4 stretching region ~1300–800 cm^{-1}, the strongest maximum composed of bands at 998, 960 and 943 cm^{-1} is attributed to the ν_1 symmetric, and the bands at 1183, 1147, 1109 and 1053 cm^{-1} to the ν_3 antisymmetric stretching vibrations (Fig. 6b). According to Frost et al. (2013), the Raman spectrum in the range 800–300 cm^{-1} (PO_4 bending region for plimerite of Sejkora et al. 2011) may be divided into four parts (Fig. 6c). The spectral hump from 650 to 850 cm^{-1} is explained by Frost et al. (2013) as a manifestation of hydroxyl deformation vibrations. The re-

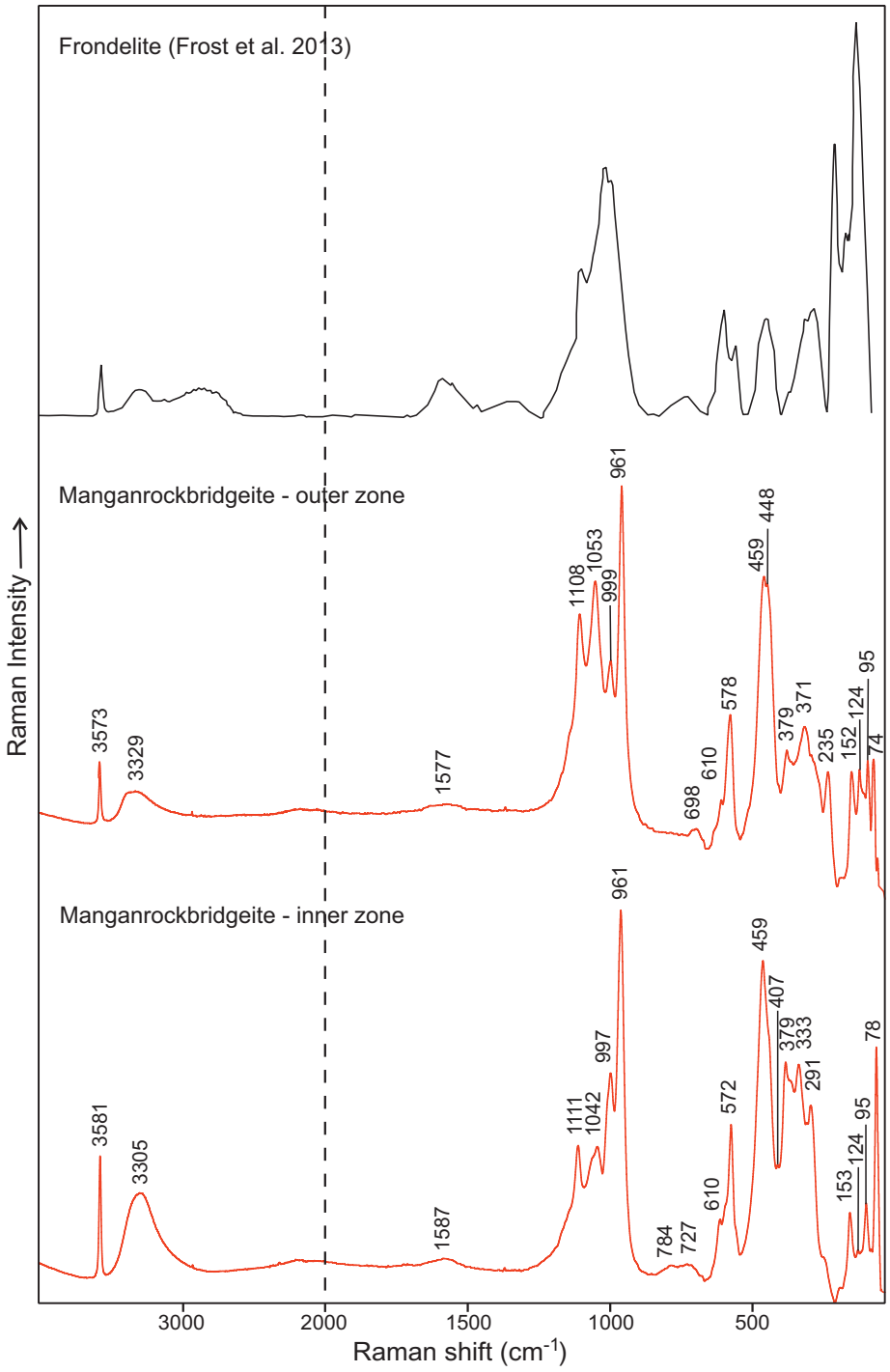

Fig. 5. Raman spectra of the outer and inner zone of manganrockbridgeite from the Jocão pegmatite in comparison with frondelite from the same locality (Frost et al. 2013); split at 2000 cm^{-1}.

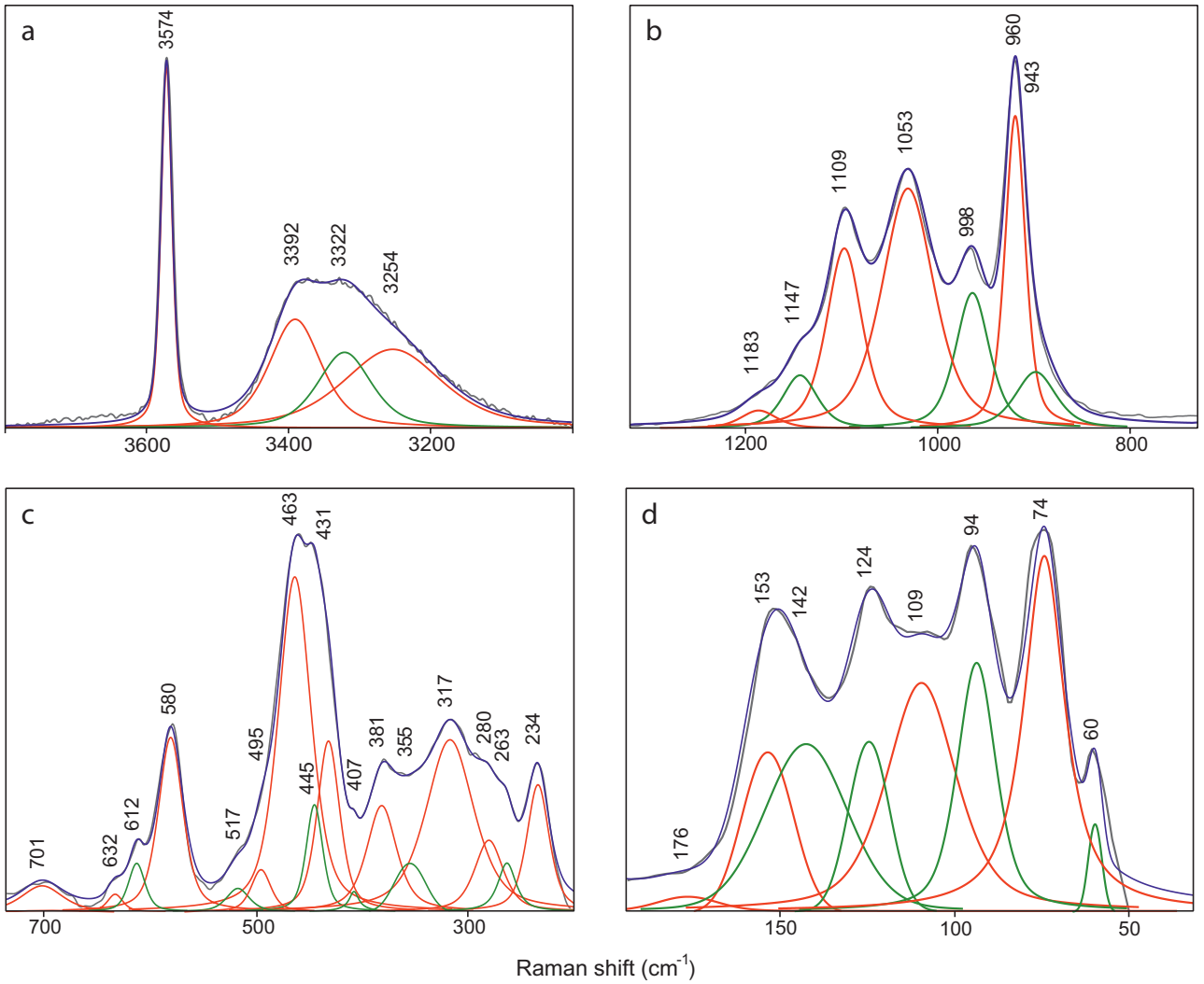

Fig. 6. Results of the band component analysis in the Raman spectrum of manganrockbridgeite from the Jocão pegmatite: **a** – OH stretching region, **b** – PO_4 stretching region, **c** – PO_4 bending and metal-oxygen vibrations region, **d** – lattice vibrations region. The cumulative curve is shown in blue, fitted bands in red and green.

solved component bands in the range of 650–550 cm^{-1} (580 cm^{-1} with shoulders at 632 and 612 cm^{-1}) are assigned to the ν_4 out of plane bending modes of the PO_4 unit. The second group of bands at 517, 495, 463, 445, 431 and 407 cm^{-1} are attributed to the ν_2 PO_4 in-plane bending modes. The third group of bands is considered to be a manifestation of vibrations of complex metal-centred polyhedra, in lower wavelengths probably influenced by lattice vibrations. Bands of *M*–O stretching (most likely at ~381–263 cm^{-1}) overlap there those of O–*M*–O symmetric bending (most likely at ~263–234 cm^{-1}) vibrations. The bands at lower wavelengths belong to external or lattice vibrations (Fig. 6d).

3.4. Chemical composition

The chemical composition of manganrockbridgeite and frondelite from the Jocão pegmatite was determined on polished and carbon-coated fragments mounted in an epoxy cylinder using a Cameca SX 100 electron microprobe (Department of Mineralogy and Petrology, National Museum Prague). The instrument was operated in wavelength-dispersive mode at an accelerating voltage of 15 keV, beam current of 10 nA, and beam diameter of 5 µm. The following X-ray lines and standards were used: *K*α lines: P, Ca (apatite), Mg (diopside), Mn (rhodonite), Fe (hematite), Zn (ZnO); *L*α lines: As (clinoclase). Contents of Al, Ba, Bi, Cl, Co, Cu, F, K, N, Na, Ni, Pb, Si, S, Sb, Sr and V were below detection limits (usually ~0.05–0.10 wt. %, 0.15 wt. % for Pb and Zn, and 0.18 wt. % for N). Counting times were 10–20 s (100 s for N) on peak and half of this time for each background position. The raw intensities were converted to the concentrations automatically using *PAP* (Pouchou and Pichoir 1985) matrix-correction procedure. Water could not be analysed directly because of the very small amount of

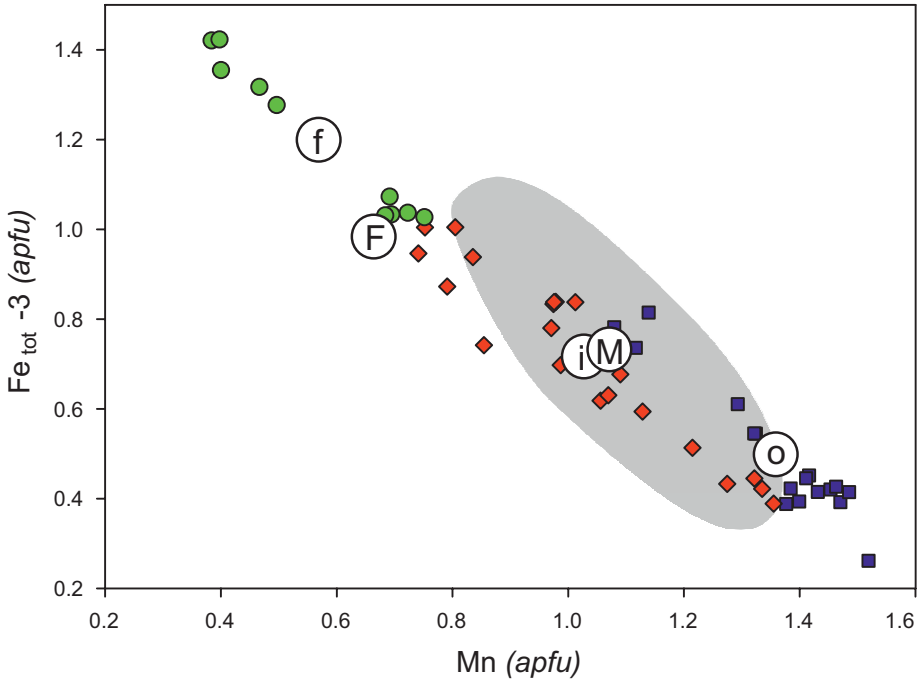

Fig. 7. Compositional range of analytical EMP points in a plot of atoms per formula unit *(apfu)* of Mn versus Fe_{tot} subtracted by 3 atoms in *M*1 + *M*3 sites. Blue squares for the outer manganrockbridgeite zone, red diamonds for the inner manganrockbridgeite zone, green circles for frondelite from two separate vugs; the shaded area indicates the range of the original manganrockbridgeite from Hagendorf-Süd (Grey et al. 2023); circles show mean values for the outer zone (o), inner zone (i), frondelite (f), type manganrockbridgeite (M) and type frondelite (F).

material available; the H_2O content was confirmed by Raman spectroscopy and calculated by the stoichiometry of the ideal formula.

A summary of analytical data for manganrockbridgeite and frondelite from the Jocão pegmatite is given in Tab. 5, the EMP point analysis are available as Supple-

Tab. 5 Ranges of compositions for manganrockbridgeite and frondelite from the Jocão pegmatite

	Manganrockbridgeite outer zone (n = 19)			Manganrockbridgeite inner zone (n = 23)			Frondelite (n = 10)		
	Mean	Range	SD	Mean	Range	SD	Mean	Range	SD
CaO (wt. %)	0.29	0.16–0.46	0.08	0.25	0.11–0.61	0.14	0.12	0.00–0.22	0.07
MgO	0.04	0.00–0.13	0.04	0.10	0.00–0.37	0.12	0.04	0.00–0.07	0.03
MnO	14.95	11.95–16.69	1.31	11.45	8.34–15.19	2.03	6.40	4.33–8.72	1.61
ZnO	0.03	0.00–0.24	0.08	0.03	0.00–0.29	0.08	0.06	0.00–0.22	0.10
FeO*	5.11	4.76–5.56	0.21	5.50	5.04–5.97	0.27	1.44	1.37–1.51	0.06
Fe_2O_3*	37.67	35.06–40.96	1.55	40.52	37.16–44.04	2.00	51.59	49.27–54.44	2.15
As_2O_5	0.09	0.00–0.43	0.12	0.06	0.00–0.41	0.11	0.14	0.00–0.43	0.14
P_2O_5	32.99	32.46–33.62	0.28	33.42	32.93–33.75	0.25	33.69	33.41–33.94	0.17
H_2O**	8.61	7.90–9.18	0.29	8.76	8.31–9.26	0.30	7.63	7.25–7.93	0.25
Total	99.78			100.09			101.11		
Ca *(apfu)*	0.034	0.018–0.053	0.009	0.028	0.012–0.070	0.016	0.014	0.000–0.025	0.008
Mg	0.006	0.000–0.021	0.007	0.016	0.000–0.058	0.019	0.005	0.000–0.011	0.005
Zn	0.003	0.000–0.019	0.006	0.003	0.000–0.023	0.007	0.005	0.000–0.017	0.007
Mn	1.359	1.079–1.519	0.121	1.027	0.741–1.355	0.180	0.569	0.384–0.751	0.145
Fe^{2+}	0.458	0.427–0.500	0.019	0.487	0.444–0.525	0.024	0.126	0.121–0.133	0.005
Fe^{3+}	0.094	0.007–0.253	0.067	0.293	0.113–0.482	0.107	0.854	0.741–0.980	0.098
□	0.047	0.003–0.126	0.033	0.147	0.056–0.241	0.053	0.427	0.370–0.490	0.049
Σ*M*2	2.000			2.000			2.000		
Fe^{3+} (*M*1+*M*3)	2.947	2.828–3.097	0.064	2.937	2.832–3.042	0.066	3.219	3.146–3.310	0.062
As	0.005	0.000–0.024	0.007	0.003	0.000–0.023	0.006	0.008	0.000–0.024	0.008
P	2.995	2.976–3.000	0.007	2.997	2.977–3.000	0.006	2.992	2.976–3.000	0.008
Σ	3.000			3.000			3.000		
$OH_{calc.}$	3.840	3.484–4.292	0.191	3.810	3.497–4.126	0.197	4.658	4.439–4.930	0.187
$H_2O_{calc.}$	1.160	0.708–1.516	0.191	1.190	0.874–1.503	0.197	0.342	0.070–0.561	0.187
Σ(OH,H_2O)	5.000			5.000			5.000		

* Based on Mössbauer spectroscopy (for manganrockbridgeite new analysis, for frondelite analogically with dark-brown type material from Sapucaia, Grey *et al.* 2019a). ** Assuming ($OH+H_2O$) = 5 in the ideal formula and equalizing charge balances.

Tab. 6 Powder X-ray pattern (*d* in Å) for manganrockbridgeite from the Jocão pegmatite compared with published data

Jocão pegmatite (this work)						Hagendorf-Süd (Grey et al. 2023)						
I_{obs}	d_{obs}	d_{calc}	*h*	*k*	*l*	I_{obs}	d_{obs}	d_{calc}	I_{calc}	*h*	*k*	*l*
						6	8.360	8.4525	5	0	2	0
45	6.988	6.991	0	0	1	21	7.010	7.0562	34	0	0	1
						61	4.880	4.8839	30	1	0	0
8	4.659	4.676	–1	1	1							
						32	4.734	4.6920	27	1	1	0
7	4.388	4.392	0	3	1			4.4032	5	0	3	1
20	4.231	4.234	0	4	0	16	4.232	4.2263	14	0	4	0
								3.6852	11	–1	3	1
48	3.619	3.622	0	4	1	32	3.638	3.6257	35	0	4	1
35	3.464	3.465	–1	0	2	71	3.458	3.4810	51	–1	0	2
100	3.423	3.423	0	1	2			3.4537	48	0	1	2
						30	3.404	3.4095	40	–1	1	2
								3.2559	5	0	2	2
48	3.219	3.214	1	2	1	100	3.209	3.2296	100	1	2	1
								3.1958	22	1	4	0
24	3.192	3.194	–1	4	1							
24	3.047	3.048	0	5	1	7	3.064	3.0491	19	0	5	1
<1	2.972	2.972	0	3	2	12	2.990	2.9903	6	0	3	2
13	2.820	2.823	0	6	0			2.8175	9	0	6	0
						26	2.784	2.7799	28	1	5	0
14	2.775	2.780	–1	5	1							
8	2.695	2.696	0	4	2	4	2.692	2.7084	7	0	4	2
5	2.5961	2.5973	–2	0	1	11	2.596	2.5990	19	–2	0	1
						70	2.435	2.4581	14	1	1	2
								2.4501	5	–1	1	3
								2.4405	46	1	6	0
27	2.4322	2.4327	–2	0	2							
								2.4253	26	–1	5	2
								2.4108	11	–2	1	2
						6	2.281	2.2849	10	0	7	1
						16	2.191	2.1900	11	–1	6	2
						4	2.172	2.1648	10	1	7	0
						6	2.141	2.1418	14	1	4	2
2	2.1193	2.1170	0	8	0	7	2.118	2.1131	7	0	8	0
						8	2.083	2.0805	8	2	1	1
								2.0728	8	–2	1	3
15	2.0409	2.0415	0	4	3	10	2.055	2.0552	6	0	4	3
						26	1.9742	1.9796	28	2	5	0
						4	1.9330	1.9394	6	1	8	0
						5	1.9212	1.9103	8	–2	6	1
3	1.9199	1.9198	0	5	3							
								1.8771	6	–1	0	4
3	1.8547	1.8544	–1	6	3	3	1.8515	1.8600	5	–1	6	3
						24	1.8494	1.8426	17	0	0	4
								1.8128	5	0	8	2
14	1.7490	1.7477	0	0	4			1.7640	7	0	0	4
						7	1.7492	1.7289	15	–1	7	3
						10	1.7280	1.7155	8	–1	4	4
1	1.7236	1.7233	–2	1	4							
2	1.7168	1.7169	2	7	0							
						11	1.7128	1.7112	9	2	2	2
						7	1.7027	1.7047	8	–2	2	4
1	1.7108	1.7101	–3	1	1							
						9	1.6891	1.6905	9	0	10	0
						16	1.6566	1.6580	12	0	9	2
10	1.6559	1.6561	–2	3	4							
1	1.6414	1.6409	–2	8	1							
14	1.6157	1.6155	0	4	4	7	1.6229	1.6279	13	0	4	4
						20	1.6094	1.6148	23	2	4	2
						49	1.5961	1.6094	20	–2	4	4
5	1.5984	1.5981	2	8	0			1.5979	17	2	8	0
								1.5923	9	–3	4	2
6	1.5663	1.5669	0	8	3			1.5719	7	0	8	3
						23	1.5508	1.5523	7	2	5	2
								1.5475	10	–2	5	4
4	1.5223	1.5215	–1	10	2							
						8	1.4909	1.4888	8	2	9	0
								1.4850	5	2	6	2
						26	1.4696	1.4674	19	–3	6	2
1	1.4630	1.4628	–3	5	3							
1	1.4049	1.4050	1	4	4							
1	1.3727	1.3732	2	4	3							

mentary Material linked to this article (ESM 3).

Similar to the original material from Hagendorf-Süd, the studied sample shows a wide range of manganese and iron contents. The outer zone is significantly richer in Mn than the inner zone where the manganrockbridgeite passes to frondelite (Fig. 7).

According to Grey et al. (2019a), grouping the divalent cations Ca, Mg, Mn and Zn as M^{2+}, the stoichiometric $A_2B_3(PO_4)_3(OH)_4(H_2O)$ formula for the rockbridgeite group minerals can be generalised as:

$$(M^{2+}_{2-x}Fe^{2+}_{x-3\delta}Fe^{3+}_{2\delta}\square_{\delta})_2Fe^{3+}_{3+y}(PO_4)_3(OH)_{4+3y}(H_2O)_{1-3y},$$

where 3δ corresponds to the amount of oxidation of Fe^{2+} in the *M*2 site and *y* represents the difference in Fe^{3+} content at sites *M*1 and *M*3 compared to $3Fe^{3+}$ *pfu*. Empirical formulae for manganrockbridgeite from the Jocão pegmatite based on this rule and analytical data given in Tab. 5 are for the outer zone:

$$(Mn_{1.36}Fe^{2+}_{0.46}Fe^{3+}_{0.09}Ca_{0.03}Mg_{0.01}\square_{0.05})_{\Sigma 2.00}Fe^{3+}_{2.95}(PO_4)_{3.00}(OH)_{3.84}(H_2O)_{1.16}$$

and for the inner zone:

$$(Mn_{1.03}Fe^{2+}_{0.49}Fe^{3+}_{0.29}Ca_{0.03}Mg_{0.02}\square_{0.14})_{\Sigma 2.00}Fe^{3+}_{2.94}(PO_4)_{3.00}(OH)_{3.81}(H_2O)_{1.19}.$$

The results of the EMP analysis show a significant chemical similarity of the inner zone of the manganrockbridgeite aggregates with the original material from Hagendorf-Süd. This is also evident from the classification diagram Mn–Fe^{2+}–Fe^{3+} for rockbridgeite-group minerals (Fig. 8). The average value for frondelite from two isolated

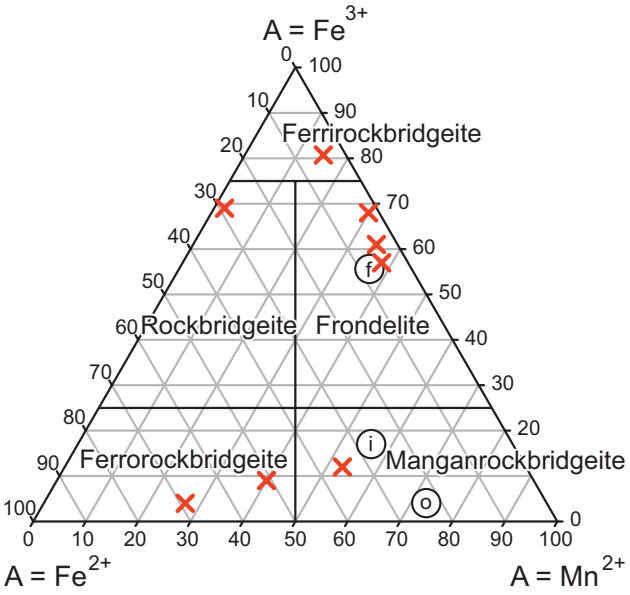

Fig. 8. Rockbridgeite-group mineral phase fields, based on the occupation of the *M*2 site by Mn^{2+}, Fe^{2+} and Fe^{3+} (Grey et al. 2019a, b). Composition of type specimens (two for ferrorockbridgeite) according to Grey et al. (2023) is marked with red crosses, circles show mean values for the outer (o) and inner zone (i) of manganrockbridgeite as well as for frondelite (f) from the Jocão pegmatite.

cavities in the studied sample is also shown for comparison.

3.5. X-ray diffraction data

Powder X-ray diffraction (P-XRD) data for manganrockbridgeite were obtained on a Bruker D8 Advance diffractometer equipped with solid-state LynxEye detector and secondary monochromator producing CuK_α radiation (Department of Mineralogy and Petrology, National Museum, Prague). The instrument was operated at 40 kV and 40 mA. In order to minimize the background, the powder samples were placed on the surface of a flat silicon wafer in acetone suspension. The powder pattern was collected in the Bragg–Brentano geometry in the range 5–70° 2θ, step 0.01° and counting time of 10 s per step (total duration of the experiment ≈ 18 hours). Positions and intensities of diffractions were processed using a pseudo-Voigt shape function with the High-ScorePlus (PANalytical) program.

Tab. 7 Unit-cell parameters of manganrockbridgeite

	Jocão pegmatite (this study)	Hagendorf-Süd Grey et al. (2023)
a [Å]	5.195(2)	5.198(2)
b [Å]	16.936(4)	16.944(5)
c [Å]	7.452(3)	7.451(3)
ß [°]	110.25(3)	110.170(9)
V [Å^3]	615.1(4)	616.0(4)

The powder diffraction data indexed for space group $P2_1/m$ in comparison with the data of Grey et al. (2023) are given in Tab. 6. Unit-cell parameters were refined by least-square method with the Celref program (Laugier and Bochu 2002) using structural data published by Grey et al. (2023) as: a = 5.195(2) Å, b = 16.936(4) Å, c = 7.452(2) Å, β = 110.25(3)° and V = 615.1(4) Å^3 (Tab. 7).

4. Conclusions

The dominant primary phosphate mineral in the Jocão pegmatite is triphylite. Triphylite crystallized during the magmatic lithium rich stage (e.g. Ginsburg 1960; Baijot et al. 2014). It occurs in two main habits in accordance with the observations of Keller (1988): dendritic and blocky, forming massive nodules if the inner internal zone along the margin of the pegmatite core (Baijot et al. 2014). Massive grey triphylite forms also the groundmass of the studied sample.

During postmagmatic hydrothermal processes, triphylite was altered and replaced by various phosphate minerals. No high-temperature hydrothermal alteration products as "ferrisicklerite" and heterosite corresponding to classic Quensel-Mason sequence (Quensel 1937; Mason 1941) were observed on the studied sample. Either these mineral phases were completely replaced, or the triphylite was altered only during the lower-tempered hydrothermal phase under non-oxidizing conditions. It is likely that the processes took place in a relatively closed system (as suggested by Baijot et al. 2014) while preserving the overall iron and manganese proportions. Thus, in the studied sample, the first product of triphylite decomposition appears to be an assemblage of correianevesite and manganoan vivianite, superposed later at lower temperature and oxidizing conditions by recrystallized collomorphic crusts of older frondelite and younger manganrockbridgeite, both separated by a poorly crystalline phase likely corresponding to kenngottite. Another two small cavities observed in the sample are completely filled with frondelite with slightly different Mn/Fe ratios, leaving no space for crystallization of manganrockbridgeite. Another member of the association, hureaulite, seems to be nearly syngenetic with the minerals of the rockbridgeite series.

In a similar association with correianevesite, pink hureaulite, hematite and kenngottite, manganrockbridgeite was described on the holotype specimen from Hagendorf-Süd. In addition, phosphates of late hydrothermal to supergene stages also occur there (Grey et al. 2023). The described manganrockbridgeite from the Jocão pegmatite is also very similar to the holotype sample in terms of chemical composition and structural data.

Acknowledgements. The authors thank the reviewers Ian E. Grey and Günther Redhammer, the editor-in-chief Vladislav Rapprich and the handling editor Martin Števko for comments and suggestions that helped to improve the manuscript. This work was financially supported by the Ministry of Culture of the Czech Republic (long-term project DKRVO 2024-2028/1.II.a National Museum, 00023272), by the Grant Agency of the Masaryk University Brno, Czech Republic (project MUNI/A/1271/2022) and by the Ministry of Education, Youth and Sports of the Czech Republic (Research Infrastructure NanoEnviCz, project No. LM2023066).

Electronic supplementary material. ESM is available online at the Journal website (http://dx.doi.org/10.3190/jgeosci.387).

References

Ardizzi JB, Atencio D (2018) Mineralogy of rockbridgeite–frondelite series and its phosphate association from the Jocão pegmatite, Galileia, Minas Gerais, Brazil. Conference Paper of the 22nd IMA Meeting Melbourne, pp 1–494

Baijot M, Hatert F, Dal Rio F, Philipo S (2014) Mineralogy and petrography of phosphate mineral association from the Jocão pegmatite, Minas Gerais, Brazil. Canad Mineral 52: 373–397

Briggs D (2003) XPS: Basic principles, spectral features and qualitative analysis. In: Briggs D, Grant JT (eds) Surface Analysis by Auger and X-ray Photoelectron Spectroscopy. IM Publications, Chichester, UK, pp 31–56

Chaves ML, Scholz R, Atencio D, Karfunkel J (2005) Assembléias e paragêneses minerais singulares nos pegmatitos de região de Galiléia (Minas Gerais). Geociencias 24(2): 143–161 (in Portugal)

Chukanov NV, Scholz R, Zubkova NV, Pekov IV, Belakovskiy DI, Van KV, Lagoeiro L, Graça LM, Krambrock K, de Oliveira LCA, Menezes Filho LAD, Chaves MLSC, Pushcharovsky DY (2014) Correianevesite, $Fe^{2+}Mn^{2+}_2(PO_4)_2 \cdot 3H_2O$, a new reddingite-group mineral from the Cigana mine, Conselheiro Pena, Minas Gerais, Brazil. Amer Miner 99: 811–816

Frondel C (1949): The dufrenite problem. Amer Miner 34: 513–540

Frost RL, Xi Y, Scholz R, Belotti FM, Beganovic M (2013) SEM-EDX, Raman and infrared spectroscopic characterization of the phosphate mineral frondelite $(Mn^{2+})(Fe^{3+})_4(PO_4)_3(OH)_5$. Spectrochim Acta A110: 7–13

Ginsburg AI (1960) Specific geochemical features of the pegmatitic process. 21st International Geological Congress Session Norden Report 17: 111–121

Grey IE, Kampf AR, Keck E, Cashion JD, MacRae CM, Gozukara Y, Shanks FL (2019a) Ferrirockbridgeite, $(Fe^{3+}_{0.67}\square_{0.33})_2(Fe^{3+})_3(PO_4)_3(OH)_4(H_2O)$, and the oxidation mechanism for rockbridgeite-group minerals. Eur J Mineral 31: 585–594

Grey IE, Kampf AR, Keck E, Cashion JD, MacRae CM, Gozukara Y, Peterson VK, Shanks FL (2019b) The rockbridgeite group approved and a new member, fer rorockbridgeite,$(Fe^{2+},Mn^{2+})_2(Fe^{3+})_3(PO_4)_3(OH)_4(H_2O)$, described from the Hagendorf Süd pegmatite, Oberpfalz, Bavaria. Eur J Mineral 31: 389–397

Grey IE, Hochleitner R, Kampf AR, Boer S, MacRae CM, Cashion JD, Rewitzer C, Mumme WG (2023) Manganrockbridgeite, $Mn^{2+}_2Fe^{3+}_3(PO_4)_3(OH)_4(H_2O)$, a new member of the rockbridgeite group, from the Hagendorf-Süd pegmatite, Oberpfalz, Bavaria. Eur J Mineral 35: 295–304

Keck E, Grey IE, MacRae CM, Boer S, Hochleitner R, Rewitzer C, Mumme WG, Glenn M, Davidson C (2022) New secondary phosphate mineral occurrences and their crystal chemistry, at the Hagendorf Süd pegmatite, Bavaria. Eur J Mineral 34: 439–450

Keller P (1988) Dendritic phosphate minerals and their paragenetic relation to the silicate minerals of pegmatites from Namibia and from the Black Hills, South Dakota, U.S.A. Neu Jb Mineral, Abh 159(3): 249–281

Kloprogge JT, Wood BJ (2020) Handbook of Mineral Spectroscopy. Elsevier, Amsterdam, pp 1–505

Laugier J, Bochu B (2002) LMGP-Suite Suite of Programs for the interpretation of X-ray experiments, ENSP/Laboratoire des Matériaux et du Génie Physique, Ecole Nationale Supérieure de Physique de Grenoble, France. Accessed on March 5, 2023, at http://ccp14.cryst.bbk.ac.uk/tutorial/lmgp/index.html

Lindberg ML (1949) Frondelite and the frondelite-rockbridgeite series. Amer Miner 34: 541–549

Mason B (1941) Minerals of the Varuträsk pegmatite. XXIII. Some iron-manganese phosphate minerals and their alteration products, with special reference to materialfrom Varuträsk. Geol Fören Förh 63(2): 117–174

Mindat.org (2023) Jocão claim, Conselheiro Pena, Minas Gerais, Brazil. Accessed on March 5, 2023, at https://www.mindat.org/loc-69153.html#autoanchor4

Moulder JF, Stickle WF, Sobol PE, Bomben KD (1995) Handbook of X-ray Photoelectron Spectroscopy: A Reference Book of Standard Spectra for Identification and Interpretation of XPS Data. Perkin-Elmer Corporation Physical Electronics Division, Minnesota, USA, pp 1–261

Pechoušek J, Jančík D, Frydrych J, Navařík J, Novák P (2012) Setup of Mössbauer Spectrometers at RCPTM, AIP Conference Proceedings 1489: 186–193

Pedrosa-Soares AC, Chaves M, Scholz R (2009) Field Trip Guide. Eastern Brazilian Pegmatite Province. 4th

International Symposium on Granitic Pegmatites, pp 1–28

Pedrosa-Soares AC, de Campos CM, Noce CM, da Silva LC, Novo TA, Roncato J, Medeiros SM, Castañeda C, Queiroga GN, Dantas E, Dussin IA, Alkmim F (2011) Late Neoproterozoic-Cambrian granitic magmatism in Araçuaí orogen (Brazil), the Eastern Brazilian Pegmatite Province and related mineral resources. Geol Soc Spec Publ 350: 25–51

Pedrosa-Soares AC, Chaves MLSC, Scholz R, Dias CH (2022) Peg2009 pre-symposium field trip guide: Eastern Brazilian pegmatite province (Minas Gerais). Estud geol 32(2): 37–51

Pouchou JL, Pichoir F (1985) "PAP" (φρZ) procedure for improved quantitative microanalysis. In: Armstrong JT (ed.) Microbeam Analysis. San Francisco Press, San Francisco, pp 104–106

Quensel P (1937) Minerals of the Varuträsk pegmatite. I. The lithium-manganese phosphates. Geologiska Fören Förh 59(1): 77–96

Redhammer GJ, Roth G, Tippelt G, Bernroider M, Lottermoser W, Amthauer G, Hochleitner R (2006) Manganoan rockbridgeite $Fe_{4.32}Mn_{0.62}Zn_{0.06}(PO_4)_3(OH)_5$: structure analysis and ^{57}Fe Mössbauer spectroscopy. Acta Crystallogr C62: i24–i28

Rhodes K (2021) Application Note: Analysis of Iron Oxidation States by XPS. Accessed on March 5, 2023, at https://www.mccrone.com/mm/application-note-analysis-of-iron-oxidation-states-by-xps/

Sejkora J, Plášil J, Filip J (2011) Plimerite from Krásno near Horní Slavkov ore district, Czech Republic. J Geosci 56: 215–229

Shirley DA (1972) High-resolution X-ray photoemission spectrum of the valence bands of gold. Phys Rev B5: 4709–4714

Tvrdý J, Plášil J, Sejkora J, Škoda R, Vrtiška L, Dolníček Z, Petr M, Veselovský F (2022) Ferroberaunite, $Fe^{2+}Fe^{3+}_5(PO_4)_4(OH)_5 \cdot 6\ H_2O$, a mixed-valence iron member of the beraunite series, from the Gravel Hill mine, Perranzabuloe, Cornwall, England. Mineral Mag 86: 363–372

Wojdyr M. (2010) Fityk: a general-purpose peak fitting program. J App Cryst 43: 1126–1128

Žák T, Jirásková Y (2006) CONFIT: Mössbauer spectra fitting program, Surf Interf Anal 38: 710–714